OPEN

Electrocochleography Latency: Correlation With Electrode Position During Cochlear Implantation

Raphael R. Andonie,[1,2] Wilhelm Wimmer,[2,3] Reto A. Wildhaber,[4,5] Georgios Mantokoudis,[2] Marco Caversaccio,[1,2] and Stefan Weder[2]

Objectives: Cochlear implant (CI) candidates increasingly exhibit some degree of residual hearing, which should be preserved despite the implantation. Today, cochlear health is monitored during CI surgery by tracking the cochlear microphonic (CM) amplitude from intracochlear electrocochleography (ECochG) measurements. However, recent studies indicate that the insertion depth of the measuring electrode must be considered to accurately interpret these signals. The acoustic path from the cochlear base to the apex induces excitation delays in deeper regions, which should be reflected in the CM measurements. In this study, we analyzed the potential of cochlear microphonic latency (CML) as an objective method for continuously tracking CI electrode position during cochlear implantation. In addition, we examined whether CML can be associated with residual hearing.

Design: We recorded intraoperative pure-tone ECochG at maximum stimulation levels from 30 CI patients to derive CML. During CI electrode insertion, ECochG was continuously recorded at the 2 stimulation frequencies of 0.5 and 0.75 kHz. After complete insertion, ECochG was measured on all evenly numbered electrodes at frequencies of 0.25, 0.5, 0.75, and 1 kHz. The electrode locations (i.e., linear insertion depth) were identified by postoperative computed tomography (CT) scans. The location of the measuring electrode during the insertion period was then calculated backward, assuming a constant insertion speed. Finally, we used a linear regression model to relate CML to linear insertion depth. In addition, we evaluated the relationship between CML and preoperative residual hearing.

Results: CML is significantly correlated to the linear insertion depth ($p < 0.001$) during and after electrode insertion (with restrictions on 0.25 kHz stimulus, presumably since the characteristic 0.25 kHz region is not within reach of the used CI electrode arrays). Despite high inter-individual variability, our results align with documented delays in the basilar membrane observed in other studies. However, we could not identify a significant association between CML and residual hearing.

Conclusions: Our study demonstrates that objectively extracted CML encodes the intracochlear electrode location in CI patients but is not directly linked to residual hearing. Consequently, CML has the potential to enhance intraoperative ECochG analysis by providing real-time tracking of electrode position. To better understand the inter-individual variations in CML, future studies with larger patient cohorts are needed.

Key words: Basilar membrane, Cochlear implant, Cochlear microphonic latency, Electrocochleography, Electrode position, Insertion depth, Residual hearing, Traveling wave.

Abbreviations: CDL = cochlear duct length; CI = cochlear implant; CM = cochlear microphonic; CML = cochlear microphonic latency; CT= computed tomography; ECochG electrocochleography; PTA = pure-tone average; SNR = signal to noise ratio.

(Ear & Hearing 2025;46;1130–1140)

INTRODUCTION

Cochlear implants (CIs) restore speech understanding in individuals with sensorineural hearing loss by electrically stimulating intact auditory nerve cells within the inner ear. With roughly one million recipients globally, CIs have become fundamental in auditory rehabilitation (Zeng 2022). Recent expansions of the criteria for CI candidacy now include individuals with significant residual hearing, which should be preserved despite the implantation (Hempel et al. 2018). Studies have shown that CI recipients retaining residual hearing achieve superior outcomes in speech perception, sound localization, and music appreciation (Gifford et al. 2013; Sheffield et al. 2015; Gantz et al. 2022). Thus, intraoperative and postoperative monitoring of cochlear health is critical for optimizing the rehabilitation outcomes for these patients (O'Leary et al. 2022).

Intraoperative real-time electrocochleography (ECochG) recorded through the CI is increasingly acknowledged as a functional monitoring tool for assessing cochlear health (Bester et al. 2022; Schuerch et al. 2022c). The cochlear microphonic (CM) potential is of particular interest due to its robustness and its correlation with outer hair cell functionality (Dallos & Cheatham 1976; Choudhury et al. 2011; Bester et al. 2023). Despite its significance, conventional analysis predominantly depends on subjective expert evaluations, focusing solely on the CM amplitude due to its direct association with residual hearing (Weder et al. 2020; Yin et al. 2021; Schuerch et al. 2022c; Andonie et al. 2024). Current CM amplitude interpretation is based on the idea, that the CM amplitude increases steadily during an atraumatic electrode insertion, as the electrode approaches the principal signal generation site, and that signal drops are strictly attributed to surgical trauma (Giardina et al. 2019; Weder et al. 2021; Lenarz et al. 2022). However, changes in CM amplitude may also stem from various other factors, including the irregular spatial distribution and density of residual functioning hair cells among CI recipients, affecting the observed ECochG amplitude patterns (Bester et al. 2017; Sijgers et al. 2023;

[1]ARTORG Center for Biomedical Engineering Research, Bern University Hospital, University of Bern, Bern, Switzerland; [2]Department of Otorhinolaryngology, Head & Neck Surgery, Inselspital, Bern University Hospital, University of Bern, Bern, Switzerland; [3]Department of Otorhinolaryngology, Klinikum rechts der Isar, Technical University of Munich, Munich, Germany; [4]School of Life Sciences, Institute for Medical Engineering and Medical Informatics, University of Applied Sciences and Arts Northwestern Switzerland, Muttenz, Switzerland; and [5]Deptartment of Information Technology and Electrical Engineering, Signal and Information Processing Laboratory (ISI), ETH Zurich, Zurich, Switzerland.

<zdoi; 10.1097/AUD.0000000000001652>

Andonie et al. 2024). These factors, along with the uncertainty regarding intracochlear measurement position during electrode insertion, significantly limit the real-time interpretation of CM amplitude. To address this challenge, recent studies have proposed cochlear microphonic latency (CML) to estimate electrode position, thereby improving the interpretation of CM amplitude based on available data (Campbell et al. 2017; Polak et al. 2022). This concept is supported by the traveling wave theory, which postulates that sound-induced deflections of the basilar membrane propagate at a finite speed from the base toward the apex of the cochlea (Békésy 1960, 2005; Robles & Ruggero 2001; Olson et al. 2012), resulting in a progressive delay in basilar membrane excitation toward the apex. Early animal studies confirmed that CML increases from the base toward the apex (Dallos & Cheatham 1971). Given that direct in vivo measurements in normal-hearing humans are challenging, basilar membrane delays have been indirectly characterized through various methodologies, including extracochlear compound action potentials, auditory brainstem responses, and adjusted ex-vivo experiments (Eggermont 1979; Janssen et al. 1989; Schoonhoven et al. 2001; Ruggero & Temchin 2007). Furthermore, CML was proposed as a direct biomarker for residual hearing in CI patients. The experiments demonstrated that a shortened CML correlates with poorer residual hearing and that CML increase was absent in regions devoid of functioning hair cell generators (Bester et al. 2020).

However, investigations of CML have been constrained by methodological limitations such as ambiguous selection criteria that may lead to selection bias, subjective data analysis prone to observer bias, and a lack of precise intracochlear measurement location. Moreover, previous studies relied on single-frequency stimulation or solely postoperative data. The present study seeks to address these limitations through the application of previously published, objective algorithms based on autonomous linear state-space models (Andonie et al. 2023). This approach enables a fully automated, observer-independent analysis, increasing objectivity and reproducibility of the results. Furthermore, this methodology incorporates predefined, data-driven inclusion criteria to enhance the transparency and reliability of the analysis.

We recorded ECochG both during CI electrode insertion in real-time and post-implantation, employing two and four stimulation frequencies, respectively. In addition, precise intracochlear measurement locations were identified using computed tomography (CT) imaging.

Using this methodological approach, this study aims to test whether objectively extracted intracochlear CML increases with insertion depth for the applied stimulation frequencies. In addition, we seek to determine whether CML and residual hearing correlate, hypothesizing that patients with better residual hearing will exhibit longer CML and larger CML increase along the linear insertion depth (LID), compared with those with poorer residual hearing.

These insights are expected to enhance our knowledge of cochlear physiology and, by integrating them with previously established inner ear parameters, increase the diagnostic value of ECochG. Ultimately, this enhanced diagnostic value could lead to more precise assessments of cochlear health, thereby improving surgical management and outcomes for CI patients.

MATERIALS AND METHODS

Patient Cohort

This prospective cohort study was conducted in accordance with the Declaration of Helsinki and the study protocol was approved by the local institutional review board (KEK-BE 2019-01578). Written informed consent was obtained from all individuals before study participation. Eligible participants were adult patients receiving a CI622 cochlear implant (Cochlear Ltd., Sydney, Australia). All implantation used a posterior tympanotomy approach, followed by electrode array insertion through the round window. In addition, patients were required to have a preoperative audiogram and to exhibit measurable ECochG responses either during or after electrode insertion, as detailed later. Both preoperative and postoperative CT scans had to be available for accurate determination of CI electrode locations. Based on these criteria, we included 30 ears from 30 individuals in this study. The demographic data of the study population are summarized in Table 1.

Residual Hearing

The day before surgery, we recorded unaided air conduction pure-tone audiograms in an acoustic chamber using a clinical audiometer (Equinox, Interacoustics A/S, Assens, Denmark) connected to insert earphones. To quantify the residual hearing, we calculated the low-frequency pure-tone average (PTA) at 0.25, 0.5, and 1 kHz. On average, the patients had a PTA of 81 dBHL with an SD of 17 dBHL. Individual PTAs are listed in Table 1.

CT and Electrode Locations

We determined intracochlear electrode locations using preoperative and postoperative CT scans. The resolution of the CT scans varied between 0.12 and 0.37 mm with a slice thickness ranging from 0.20 to 1.50 mm. Based on manual landmark selection, a reference coordinates system was computed for each cochlea followed by a robust modiolar axis detection on the preoperative scans (Verbist et al. 2010; Wimmer et al. 2019). We used manually selected cochlear base length A and width B to estimate the cochlear duct length

$$\mathrm{CDL} = 1.71 \cdot \left(1.18A_{\mathrm{oc}} + 2.69B_{\mathrm{oc}} - \sqrt{0.72A_{\mathrm{oc}}B_{\mathrm{oc}}}\right) + 0.18 \text{ mm}$$

along the organ of Corti with $A_{\mathrm{oc}} = A - 1$ mm and $B_{\mathrm{oc}} = B - 1$ mm (Alexiades et al. 2015; Schurzig et al. 2018; Rathgeb et al. 2019; Alshalan et al. 2022; Schraivogel et al. 2023b). For all electrodes, we computed the angular insertion depth and LID in the reference coordinate system from the Cartesian electrode locations. The electrode positions were visually labeled in the postoperative scans that were co-registered with the preoperative scans (Schraivogel et al. 2023a). To compare the CMLs with prior studies, we calculated the characteristic frequency

$$F_c\,(\mathrm{LID}) = 165.4\mathrm{Hz}\left(10^{\frac{2.1(\mathrm{CLD}-\mathrm{LID})}{\mathrm{CLD}}} - 0.88\right)$$

for a given LID based on the individual CDL (Greenwood 1990).

TABLE 1. Demographics of the study population

ID	Sex	Side	Course	Etiology	Age* (yr)	CDL† (mm)	CF‡ (Hz)	LID§ (mm)	PTA¶ (dBHL)
ID-01	M	R	S	T	43	36.8	864	23.0	82
ID-02	F	R	S	U	69	35.5	1393	19.2	88
ID-03	F	R	P	EH	42	30.9	412	23.2	88
ID-04	M	L	P	EH	57	32.0	506	22.9	68
ID-05	M	R	P	U	76	35.2	944	21.5	70
ID-06	F	L	P	U	62	31.0	660	20.8	112
ID-07	M	R	P	U	90	33.3	782	21.4	112
ID-08	F	R	P	U	56	33.1	729	21.7	112
ID-09	F	R	S	U	40	34.7	805	22.2	78
ID-10	M	R	P	U	78	32.9	521	23.4	62
ID-11	F	R	P	U	48	30.6	513	21.9	105
ID-12	F	R	P	EH	62	33.1	516	23.6	73
ID-13	F	R	P	U	59	33.9	1327	18.6	70
ID-14	F	L	P	OS	72	32.3	650	21.8	85
ID-15	M	L	S	U	68	35.0	667	23.5	73
ID-16	F	R	P	U	70	30.3	451	21.2	111
ID-17	F	R	P	U	87	32.1	946	19.6	100
ID-18	F	L	P	OS	82	32.3	1280	19.7	68
ID-19	M	L	P	EH	38	34.0	982	22.6	75
ID-20	F	R	S	U	60	31.8	748	21.0	82
ID-21	M	R	P	U	29	35.0	943	21.4	65
ID-22	F	R	P	U	65	35.5	897	22.0	48
ID-23	M	R	P	U	85	34.0	1251	19.0	75
ID-24	M	L	P	EH	62	36.8	1015	22.0	73
ID-25	M	L	P	U	71	32.1	532	22.7	78
ID-26	F	R	P	U	40	31.8	657	19.9	84
ID-27	M	R	P	U	57	31.7	605	22.7	68
ID-28	M	L	P	OS	80	31.2	834	23.7	58
ID-29	F	R	S	U	38	31.1	552	21.9	85
ID-30	F	L	P	U	54	32.1	583	22.2	94
Mean					64	33.1	743	22.0	81

Calculated from hearing thresholds at 0.25, 0.5, 0.75, and 1.0 kHz.
**Age at surgery.*
†Cochlear duct length.
‡Characteristic frequency place of most apical electrode.
§Linear insertion depth of the most apical electrode in degrees.
¶Pure-tone average (preoperative).
EH, endolymphatic hydrops; OS, otosklerosis; P, progressive sensory-neural hearing loss; S, sudden sensory-neural hearing loss; T, trauma; U, unknown.

Intraoperative ECochG

For acoustic stimulation, we interfaced the acoustic component of a Nucleus 6 hybrid sound processor (Cochlear Ltd., Sydney, Australia) to a sterile 25 cm long sound delivery tube with a mounted foam eartip (ER3-21 and ER3-14A; Etymotic Research Inc., Elk Grove Village, IL, USA), which had been separately sterilized using hydrogen peroxide vapor low-temperature plasma (STERRAD 100NX, Advanced Sterilization Products [ASP], Irvine, CA, USA). The sound tube was placed in the patient's outer ear canal before surgical incision (Schuerch et al. 2022a, b). Intraoperative ECochG was recorded through the CI using the *Cochlear Research Platform* software version 2.0 (Cochlear Ltd.). We applied alternating condensation and rarefaction stimuli lasting 11 msec with a rise and fall time of 1 msec. The recording window was set to 16 msec with a sampling rate of 20.5 kHz. The ECochG measurements encompassed two protocols:

a. Continuous recording during insertion at the most apical electrode: Alternating epochs for 0.5 and 0.75 kHz stimuli were obtained every 0.7 seconds from the start until full insertion. We selected these stimulation frequencies because their tonotopic location is apical, and they are frequently used intraoperatively (Skarzynski et al. 2014; Saoji et al. 2023).
b. Measurements after complete insertion on all 11 evenly numbered electrodes, referred to as electrode sweeps: Measurements were carried out with 0.25, 0.5, 0.75, and 1 kHz stimuli. For each epoch, 30 responses were averaged to improve the signal to noise ratio (SNR).

The stimulation levels for the ECochG protocols are summarized per stimulus frequency, together with the number of averages used in Table 2.

We calculated the difference signal by subtracting the rarefaction from the condensation epoch and dividing it by two. Subsequently, we applied a 5th-order Butterworth band pass filter with a lower cutoff frequency of 0.125 kHz and an upper cutoff frequency of 8 kHz. The filter was applied in a forward-backward manner, leading to a 10th-order zero-phase filter.

TABLE 2. Intraoperative ECochG measurement protocols

	Stimulus Level in dBHL				
Protocol	0.25 kHz	0.5 kHz	0.75 kHz	1 kHz	N^*_{avg}
Continuous	n/a	108	114	n/a	1
Electrode sweep	112	108	114	115	30

**Number of averaged responses per epoch.*
ECochG, electrocochleography.

The CML was extracted by applying the method described by Andonie et al. (2023). In this method, a sinusoid with the frequency and windowing of the acoustic stimulus (representing the CM response) is fitted to the observation in a sliding window using the least-squares optimum. The CML is identified as the time (window shift), where the model best fits the observation (see section F in Wildhaber et al. 2018), which coincides with minimizing the SNR. Altogether, this is a basic least-squares problem applied in the form of a sliding window, which can be efficiently calculated using autonomous linear state-space models (Wildhaber et al. 2018; Andonie et al. 2023). In our study, the minimum response detection level was set to an SNR of 0.25 (or −12 dB), estimated using the squared error ratio between the response and a null model (Wildhaber et al. 2018).

We calculated the CML increase along the LID for each patient using the slope of a linear regression model if three or more samples were available in a measurement. Similarly, CML elevation was calculated using the intercept of the same model. This was equally done for the insertion and postinsertion data.

Statistical Analysis and Reference Data

We assessed the relationship of CML with LID using linear regression. The correlation was evaluated using Pearson's correlation coefficient r. To investigate the relationship between CML and the residual hearing of individual patients, we used Spearman's ranked correlation ρ to avoid assumptions about the statistical distribution of the data or the linearity of the relationship. In both cases, significance of the correlation was determined by the p value of the model slope ($p < 0.05$). All statistical analyses were performed using the *Python* programming language version 3.10.12 and the *statsmodels* module version 0.14.0 (Seabold & Perktold 2010).

To extract numerical reference data from other authors' previous study, we used the open-source computer vision software *WebPlotDigitizer* (Rohatgi 2024). Curve fits were reproduced using the *Python* module *Scipy* version 1.11.1 (Virtanen et al. 2020).

RESULTS

Cochlear Duct Length and Electrode Locations

The measured CDL ranged from 30.0 to 37.4 mm with a mean of 33.1 mm. The mean LID of the electrode arrays was 21.7 mm with an SD of 1.4 mm. Individual LIDs of the electrode arrays are summarized in Table 1. In our cohort, the lowest characteristic frequency reached was 0.38 kHz, as estimated using the Greenwood function. On average, the electrodes were inserted until the 0.74 kHz region with an SD of 0.26 kHz.

Intraoperative ECochG

The electrode array insertions lasted between 84 and 227 seconds, with an average of 152 seconds until completion. An illustrative example of intraoperative CML measurements for a single patient is presented in Figure 1. CM response approximations and corresponding CMLs obtained using our objective algorithms are shown for individual epochs of the postinsertion electrode sweeps.

The CML data extracted from the real-time measurements during electrode insertion had an average of 1.9 msec with an SD of 0.6 msec. The average postinsertion CML was 2.0 msec, with an SD of 1.1 msec.

CML and LID

Linear regression analysis revealed a significant positive association between CML and LID, both during and after electrode insertion. This association was evident in the insertion data for both 0.5 kHz ($r = 0.55$, $p < 0.001$) and 0.75 kHz ($r = 0.34$, $p < 0.001$), as well as in the postinsertion data for 0.5 ($r = 0.5$, $p < 0.001$), 0.75 ($r = 0.4$, $p < 0.001$), and 1 kHz ($r = 0.49$, $p < 0.001$). The post-insertion measurement at 0.25 kHz did not reveal a statistically significant relationship ($r = 0.04$, $p = 0.66$).

To compare CML during and after CI electrode insertion, we analyzed the measurement frequencies common to both protocols (i.e., for 0.5 and 0.75 kHz stimuli). During insertion, the CML at the round window was 1.33 msec. In the post-insertion measurements, this offset was 0.84 msec. At the most apical electrode position (LID = 25 mm), the CML was comparable for both protocols, showing values of 2.52 and 2.58 msec, respectively. The total increase over the 25 mm length was slightly smaller during insertion (1.18 msec) than post-insertion (1.74 msec). Consequently, the average CM signal propagation speeds were 18 to 25 m/sec during insertion and 14 to 16 m/sec postinsertion. Postinsertion CML at 1 kHz increased similarly to the 0.5 and 0.75 kHz measurements but had a shorter offset of 0.39 msec at the round window. In contrast with these results, postinsertion CML at 0.25 kHz showed no correlation with LID, with values scattered around 3 msec. The results of the statistical analysis, including the number of patients and samples used, are summarized in Table 3. Raw CML measurements and linear regression model outputs are plotted in Figure 2.

To validate our results, we compared the CMLs with human basilar membrane delays reported in earlier studies, each of which were determined using different methods: (i) similar CM-based in-situ CI recordings from a smaller cohort by Campbell et al. (2017), (ii) estimates from brainstem responses in normal-hearing individuals by Janssen et al. (1989), and (iii) signal-front delays proposed by Ruggero and Temchin (2007) for normal-hearing individuals, which were derived based on optical phase measurements in postmortem data (Von Bekesy 1943). For this purpose, we mapped the measurement locations to the individual functional map (characteristic frequency) of each cochlea and calculated the population averages of the CML. Near the round window, the average CML curves were situated around 1.1 msec (except for the 0.25 kHz measurements, as previously noted). As suggested by Campbell et al., we subtracted this value from our CML data for comparison with the basilar membrane delays. In our study, the CML progressively increased in the basal region up to approximately 1 kHz, before plateauing in the most apical part of the cochlea. This pattern was observed in the 0.5 kHz measurements during insertion and in the 0.5, 0.75, and 1 kHz measurements postinsertion. The measurements at 0.75 kHz during insertion rose to a comparable value without exhibiting a plateau in the apical region. All curves are shown in Figure 3.

Despite some variations, our measurements were close to the traveling wave delays reported by Campbell et al. (2017). Especially for characteristic frequency locations above the 1 kHz region, our CML data agreed well with the model provided by

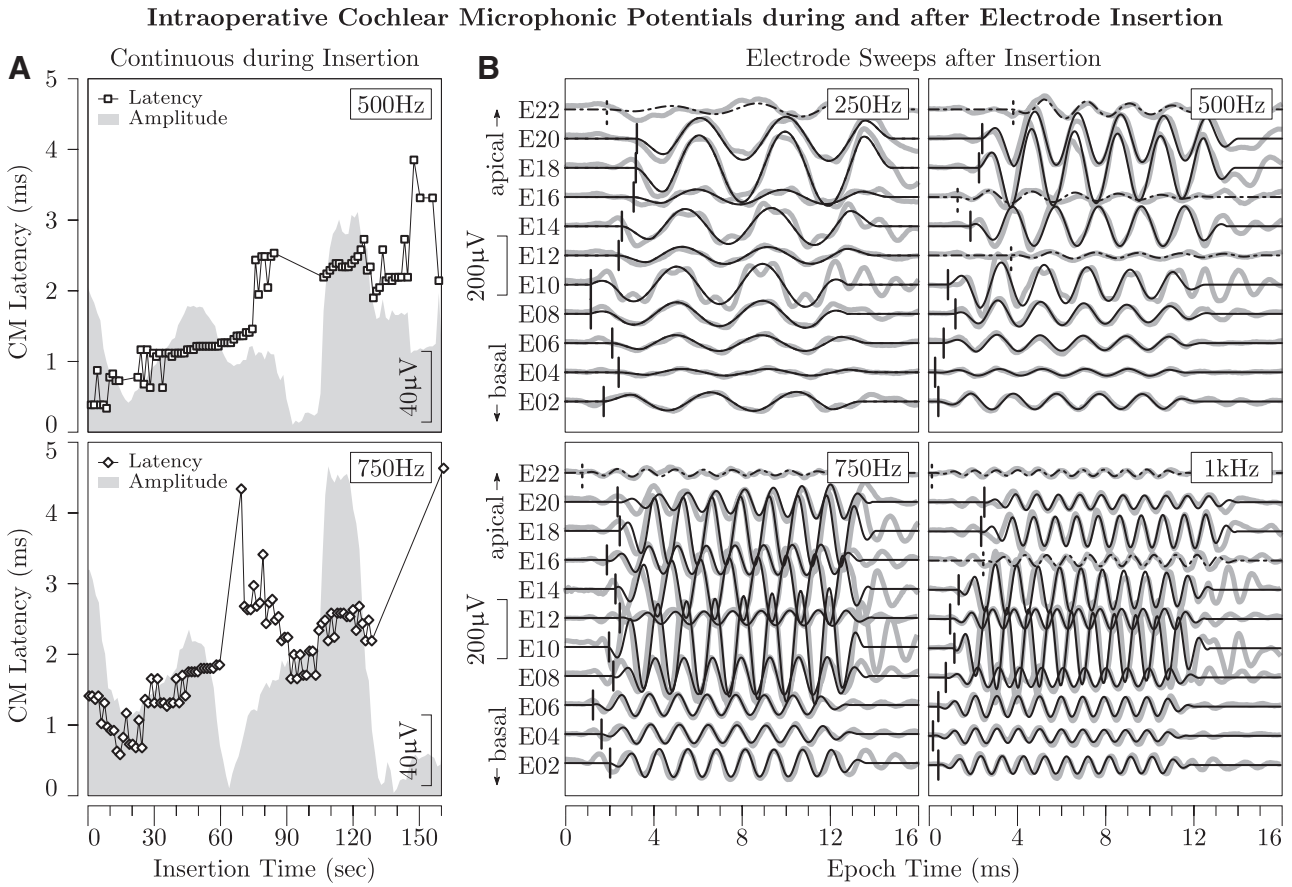

Fig. 1. Intracochlear electrocochleography recorded during CI surgery (patient ID-21). Each panel displays data corresponding to a distinct acoustic stimulation frequency, indicated in the small boxes located in the upper corners of the panels. A, CML during insertion (connected markers), recorded using the most apical CI electrode. The course of the CM amplitude is shown in the background in gray. B, Electrode sweeps measured after complete insertion at the 11 evenly numbered intracochlear CI electrodes. The raw measurements (gray) are superimposed with the CM response estimates (black) generated by our algorithm. The corresponding estimated CMLs are marked by vertical lines. The model outputs for signals below the detection threshold are shown as dashed lines. CI indicates cochlear implant; CML, cochlear microphonic latency.

TABLE 3. Cochlear microphonic latency dependence on linear insertion depth

	F (kHz)$_{stim}$	Intercept (ms)*	Slope (µsec/mm)	Slope^{-1} (m/sec)	N_p†	N‡	r	p
Insertion	0.5	1.22	55	18	13	606	0.55	<0.001
Insertion	0.75	1.45	40	25	16	545	0.34	<0.001
Postinsertion	0.25	2.81	7	143	20	141	0.04	0.657
Postinsertion	0.5	0.72	73	14	21	119	0.50	<0.001
Postinsertion	0.75	0.96	67	15	27	170	0.40	<0.001
Postinsertion	1	0.39	64	16	14	72	0.49	<0.001

*Acoustic stimulation frequency.
†Number of patients.
‡Number of observations.

Campbell et al., while having a shorter latency for frequencies below. The 0.25 kHz measurement in our study, which did not show an association between CML and LID, had elevated values that matched the most apical values reported by Campbell et al.

When compared with the traveling wave delays found by Janssen et al. (1989), our CML data demonstrated a similar increase in the basal region for characteristic frequency locations below the 1 kHz region. However, the data from Janssen et al. showed a much steeper increase in the apical region, where our measurements stagnated or even slightly sank.

Regarding the adjusted ex-vivo basilar membrane signal-front delays, found by Ruggero and Temchin (2007), our CMLs showed a total shift from the base to the apex that aligned with those findings. However, in the basal region, the model of Ruggero and Temchin remains flat until 2 kHz, whereas our measurements start increasing immediately after the round window. Specifically, in the post-insertion measurements at 0.5 and 0.75 kHz, our CML curves appeared to resemble the patterns found by Ruggero and Temchin but were skewed or shifted toward the cochlear base.

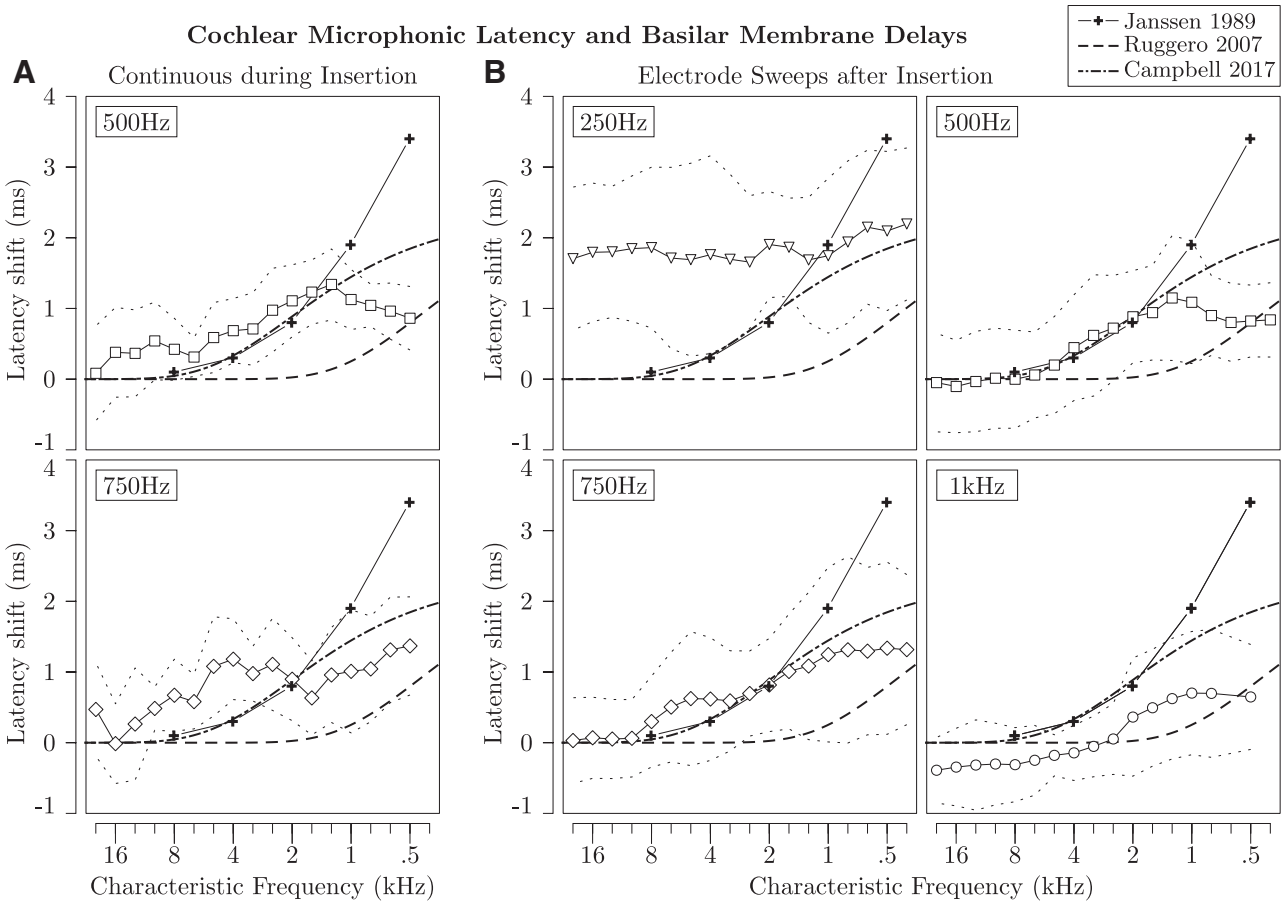

Fig. 2. Scatter plots illustrating the relationship between CML and linear insertion depth. Each panel displays data corresponding to a distinct acoustic stimulation frequency, indicated in the small boxes located in the upper corners of the panels. Linear regression results are shown with thick lines, while their 95% confidence intervals are depicted with thin lines. A, Continuous recordings during electrode array insertion. B, Post-insertion electrode sweeps and recorded immediately after electrode array insertion. CML indicates cochlear microphonic latency.

CML and Residual Hearing

The CML increased in the majority of measurements (67 of 93 cases). The average CML increase was 0.1 sec/m with an SD of 0.2 sec/m. The mean CML elevation was 1.4 msec with an SD of 2.4 msec. In our data, statistical analysis revealed no significant correlation between CML and residual hearing, whether examining CML elevation or CML increase. This lack of correlation was consistent across measurements taken both during and after CI electrode insertion. The results of the statistical analyses are given in Tables 4 and 5.

DISCUSSION

We applied our previously described objective algorithm for CM response detection and CML extraction to intraoperative ECochG measurements, acquired both during and after electrode insertion (Wildhaber et al. 2018; Andonie et al. 2023). The combination of objective CM estimation and robust electrode location retrieved from CT scans is essential for reliably assessing CML, as they help overcome previous constraints such as selection bias, manual data analysis, and enable consideration of intracochlear measurement positions. Using this methodology, we found a statistically significant association between CML and electrode insertion depth. In our dataset, the CML did not correlate with preoperative residual hearing.

Cochlear Microphonic Latency

Our results indicated that the CML increases from the cochlear base to the apex in CI patients, both during and after electrode array insertion. This correlation was significant for all stimulation frequencies (0.5, 0.75, 1 kHz), except 0.25 kHz.

In our measurements, the CML showed high inter-patient variability, as previously described by Polak et al. (2022). Remarkably, the CML at 0.25 kHz stimulation did not correlate with the LID, being broadly scattered around an average of 3 msec. We suggest that this is mainly attributed to the deep tonotopic location of 0.25 kHz within the cochlea. The electrode arrays implanted in this study achieved a minimum characteristic frequency of 0.38 kHz. As a consequence, the primary signal generators for 0.25 kHz are located beyond the measurement range covered by the electrodes. Basilar membrane deflections get smaller and defocus with increasing distance from the tonotopic location (Robles & Ruggero 2001). Thus, the constant elevation of CML at 0.25 kHz suggests that deep CM responses predominate the recordings across all electrodes. Such predominance is thought to arise when local responses in the basal region are absent because of poor high-frequency hearing, as it is typical for sensorineural hearing loss (Janssen et al. 1989; Bester et al. 2020).

For the higher stimulation frequencies, the intracochlear CML in CI patients could be explained by traveling wave

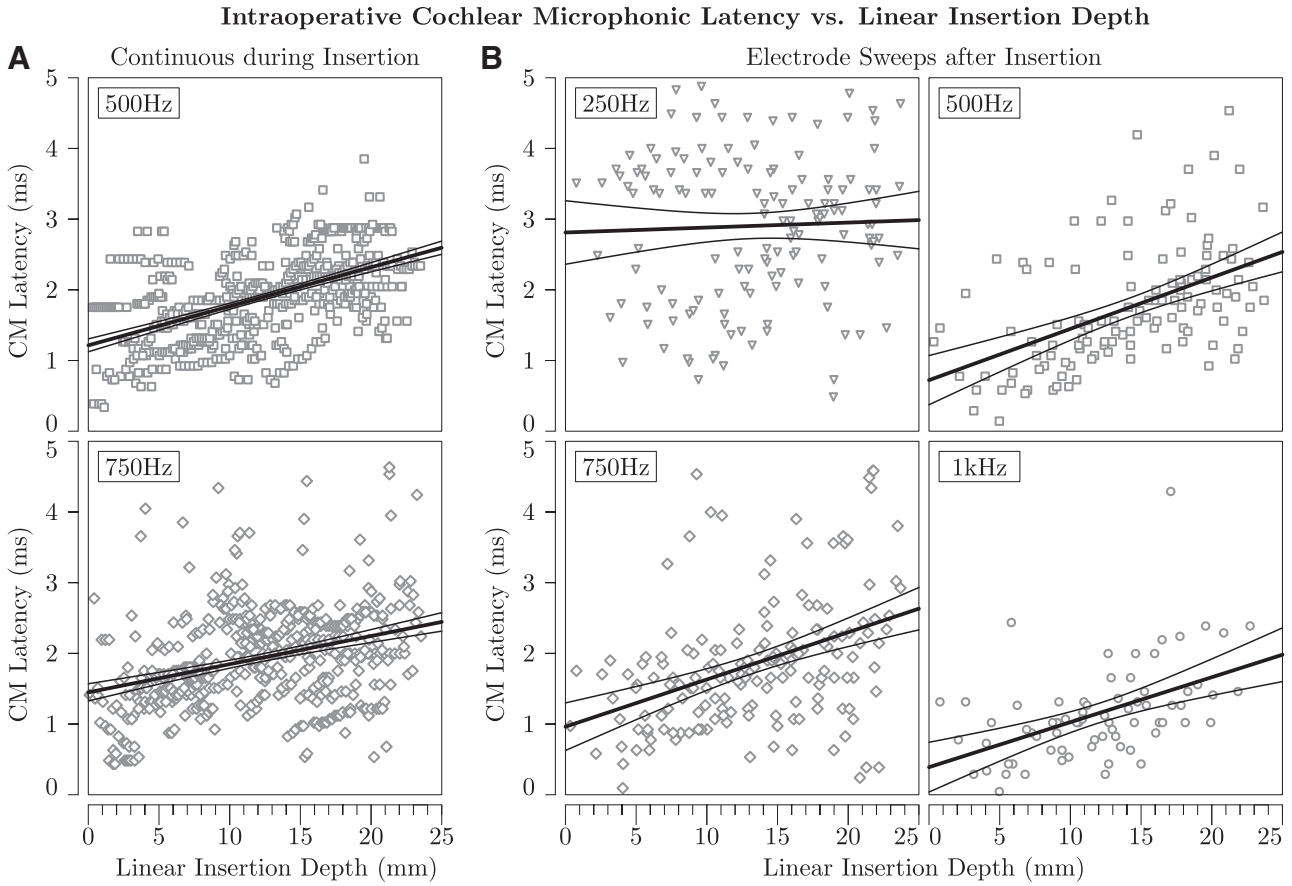

Fig. 3. Comparison between CML and basilar membrane delays retrieved from previous studies. Each panel displays data corresponding to a distinct acoustic stimulation frequency, which is indicated in the small boxes located in the upper corners of the panels. Shown are the CML population averages (markers) together with 1 SD (dotted lines). Besides the measurements, the three reference curves are also shown in each panel. A, Continuous recordings during electrode insertion. B, Data from post-insertion electrode sweeps is shown and recorded immediately after electrode insertion. CML indicates cochlear microphonic latency.

TABLE 4. Cochlear microphonic latency increase vs. preoperative hearing

	F^*_{stim}(kHz)	N†	r	p
Insertion	0.5	13	–0.16	0.60
Insertion	0.75	15	–0.16	0.57
Postinsertion	0.25	17	–0.05	0.86
Postinsertion	0.5	17	–0.11	0.67
Postinsertion	0.75	23	–0.32	0.14
Postinsertion	1	9	–0.20	0.60

**Acoustic stimulation frequency.*
†Number of observations (patients).

TABLE 5. Cochlear microphonic latency elevation vs. preoperative hearing

	F^*_{stim} (kHz)	N†	ρ	p
Insertion	0.5	13	–0.16	0.60
Insertion	0.75	15	0.01	0.57
Postinsertion	0.25	17	0.01	0.96
Postinsertion	0.5	17	0.04	0.96
Postinsertion	0.75	23	0.09	0.89
Postinsertion	1	9	0.27	0.49

**Acoustic stimulation frequency.*
†Number of observations (patients).

delays. The CML increased slower during the insertion than in the post-insertion protocol, while no substantial difference across stimulation frequencies could be observed. Using the inverse slopes of the linear regression, we estimated average CM propagation speeds from our measurements. These propagation speeds ranged from 18 to 25 m/sec during and 14 to 16 m/sec after electrode insertion, aligning with average traveling wave propagation speeds of 16.6 and 22 m/sec found in previous studies (Ruggero 1994; Polak et al. 2022). However, the CML reached a similar maximum in the apex for both protocols, indicating that the difference in propagation speed was dominated by the basal CMLs, which were slightly higher in the insertion measurements. Thus, we hypothesize that the propagation on the basilar membrane was not fundamentally changed by the insertion of the electrode array (e.g., persistent basilar membrane fixation). Further studies would be necessary to increase our understanding of the influence of the CI electrode array on mechanical wave propagation within the cochlea.

We compared the CML population averages with basilar membrane delays retrieved from previous studies (Janssen et al. 1989; Ruggero & Temchin 2007; Campbell et al. 2017). As suggested by Campbell et al. (2017), we subtracted the CML offset near the round window (1.1 msec) from our data for the comparison with the reference curves (Fig. 3). It is interesting that

1.1 msec coincides with the traveling wave delay obtained using CM at the very base of the cochlea, reported by Polak et al. (2022). It is worth noting that this is close to previously reported neural delays in the cochlea (Ruggero & Rich 1987; Robles & Ruggero 2001). A possible explanation is the presence of neural contributions in the basal ECochG measurements, as the CM is not perfectly isolated by subtracting the rarefaction from the condensation recordings (Forgues et al. 2014; Abbas et al. 2017; Bester et al. 2020; Polak et al. 2022). Another factor that may contribute to the elevated CML in the basal region is the high stimulation intensity used in this study. Loud stimuli reduce spatial selectivity within the cochlea and are associated with a basal shift of the CM amplitude maximum (Russell and Nilsen 1997; Bester et al. 2017). This effect may cause the measuring electrode near the round window to detect signals originating from more apical regions of the cochlea, exhibiting longer CML.

For characteristic frequency locations above the 1 kHz region, the CML curves agreed well with traveling wave delays derived using auditory brainstem responses from normal-hearing subjects provided by Janssen et al. (1989). In the apical region, on the other hand, the CML in our study remained much shorter than those traveling wave delays. A similar discrepancy was observed by Campbell et al. (2017), whose in-situ measurements in CI patients using a 0.5 kHz stimulus aligned well with our data. Bester et al. (2020) provided a viable explanation for this discrepancy by demonstrating the correlation between shorter CML in the apical region and poor hearing thresholds in CI patients.

We also compared our data to the much shorter signal-front delays in the basilar membrane provided by Ruggero and Temchin (2007), which were derived from postmortem experiments. In this case, our CMLs aligned with the reference data at the most basal and apical measurement locations, while being elevated in the middle region. This increase may be attributed to an overrepresentation of apical CM responses in the measurements, as might be expected in CI patients with typical high-frequency hearing loss (Eggermont 1979; Calloway et al. 2014; Bester et al. 2020, 2023; Carlson 2020).

To summarize, CML provides significant information about the measurement location. Our data was comparable to the results of previous studies, despite methodological differences (Janssen et al. 1989; Ruggero & Temchin 2007; Campbell et al. 2017). Our method for calculating signal latency provided increased certainty regarding the evaluated signal component, without relying on manual labeling (Wildhaber et al. 2018; Andonie et al. 2023). However, numerous influencing factors can potentially affect those measurements, leading to considerable variability in the data.

Association With Residual Hearing

In contrast with its dependence on intracochlear measurement location, the relationship between CML and residual hearing remains less clear. Linear regression analysis showed no statistically significant association between CML and residual hearing. This result agrees with the notion that traveling wave propagation is mainly attributed to passive cochlear mechanics (Ruggero & Temchin 2007; Polak et al. 2022). However, CM potentials in general are directly related to residual hearing (Koka et al. 2017; Bester et al. 2023; Andonie et al. 2024). Given this relationship, it seems reasonable to consider that CML might be at least indirectly influenced by residual hearing. In their analysis, Bester et al. (2020) found that CML was shorter in patients with poor residual hearing, and that local CML did not increase in cochlear regions devoid of outer hair cells. In our patients, the exact cause of hearing impairment could not be determined. In addition, at this stage, we only considered robust CM responses to accurately extract the CML, thereby focusing on measurements representing functioning hair cell regions. Therefore, no definitive conclusion can be drawn about the association between CML and residual hearing at this point.

Implications and Relevance

At present, the functional monitoring of the inner ear using ECochG predominantly depends on the examination of the CM amplitude (Dalbert et al. 2015; Weder et al. 2021). However, the measured CM amplitudes highly vary under the influence of factors such as residual hearing and proximity of the measuring electrode to the physiologic generators (Giardina et al. 2018; Weder et al. 2020; Schuerch et al. 2023). Therefore, accurate interpretation of these signals necessitates a thorough understanding of the intracochlear measurement location (Bester et al. 2017; Schuerch et al. 2022c, 2023; Andonie et al. 2024). Thus, CML-based insertion depth estimation during CI surgery can potentially be used to improve the interpretation of CM amplitude changes for functional monitoring while also providing real-time feedback to ensure correct electrode placement (Campbell et al. 2017; Polak et al. 2022).

In this study, we found an association between LID and objectively extracted CML in both real-time and post-insertion ECochG measurements for commonly used acoustic stimulation frequencies. These findings are crucial for advancing ECochG-based software for automated real-time tracking of electrode position with the goal to improve functional monitoring and electrode placement during CI surgery.

Beyond that, current methods for estimating electrode positions using the CI hardware mainly apply electrical impedance (Schraivogel et al. 2023b). However, real-time ECochG and impedance can only be recorded quasi-simultaneously using alternating measurements (Andonie et al. 2023). Therefore, CML could enhance the temporal resolution and accuracy of electrode position tracking in combined ECochG and impedance measurements.

As illustrated by the postoperative measurements of the example patient (Fig. 1B), CML and CM phase can evolve independently. In this case, the CM for 0.5, 0.75, and 1.0 kHz showed an abrupt phase inversion between the intracochlear electrodes 10 and 14 without a substantial change in latency. Thus, we suspect that these lower CM amplitude at electrode 10 could be attributed to negative interference. A comparison with the amplitude patterns during insertion (Fig. 1A) shows a similar pattern, with lower amplitudes between 60 and 90 seconds in the 0.75 and 0.5 kHz measurements, respectively. The latency fluctuations in this range are likely attributed to reduced signal quality, while the overall CML trend remains relatively stable. Previous studies have suggested that transient basilar membrane fixation by the electrode carrier might influence the ECochG patterns, which may also be relevant in the presented case (Bester et al. 2023). This highlights the limitations of single-feature CM analysis and the potential of CML to improve CM amplitude and phase interpretation in the context of clinical applications, such as hearing preservation and

verification of electrode position, especially in cases without an apical peak in the CM amplitude (Bester et al. 2017; Koka et al. 2018; Giardina et al. 2019; O'Leary et al. 2020; Andonie et al. 2024).

Finally, the analysis of CML could be used to distinct small CM responses and vibration artifacts of the electrode carrier under high stimulation levels. Similar to actual CM potentials, these artifacts resemble the acoustic stimulus, but lack any delay caused by basilar membrane transmission (Teschner et al. 2012). Using the presented algorithms, small signals with zero latency could be identified as artifacts, even though showing a good match with the expected CM waveform.

LIMITATIONS AND FUTURE DIRECTIONS

The manual insertion of the CI electrode arrays resulted in considerable variability in insertion times, leading to uncertainty in determining the exact electrode position during the insertion process, limiting comparability with the post-insertion measurements (Wimmer et al. 2024). As a result, the precise CML patterns during insertion can be distorted, limiting comparability with the postinsertion measurements. Besides that, two main factors challenge the direct translation of our findings into a prediction model for individual patients. These are (i) accurate determination of CML requires high signal-to-noise ratio, and (ii) CML showed high variability across patients. Addressing these limitations, we propose to investigate the relationship between residual hearing and CML using our objective algorithms in a larger patient cohort, since most of the patients in this study did not show a clinically relevant degree of residual hearing. This will be particularly important, as previous studies could find a relationship between CML and residual hearing (Bester et al. 2020). These results would deepen our understanding of the factors causing high variability in CML data. Finally, this knowledge could be used for the development of a patient-specific, CML-based prediction model for intracochlear electrode location.

CONCLUSION

By using objective algorithms, we were able to perform a fully automated analysis of ECochG signals, measured both during and after CI electrode insertion. In addition, we aligned the data with intracochlear electrode locations derived from CT scans. Based on this, we found a significant correlation between CML and LID, which may be attributed to traveling wave delays.

Thus, CML-based insertion depth estimation during CI surgery has the potential to enhance the interpretation of other CM parameters, such as amplitude changes for functional monitoring, and can further be used to ensure correct electrode positioning.

ACKNOWLEDGMENTS

This work was supported in part by Cochlear Ltd., Sydney, Australia, and the Department of Otorhinolaryngology of the Bern University Hospital, Inselspital.

R.R.A.: Conceptualization, methodology, formal analysis, measurements and data curation, writing-original draft; W.W.: Conceptualization, methodology, measurements and data curation, formal analysis, writing-review and editing; R.A.W.: Methodology, writing-review and editing; G.M.: Measurements, writing-review and editing; M.C.: Resources, writing-review and editing; S.W.: Conceptualization, supervision and project administration, measurements, writing-original draft. All authors contributed to the article and approved the submitted version.

This study was conducted in accordance with the Declaration of Helsinki and has been approved by the local institutional review board (KEK-Bern, Switzerland. BASEC number 2019-01578).

The measurement data would be made available upon request to the authors after a formal data sharing agreement has been reached.

The authors have no conflicts of interest to disclose.

Address for correspondence: Raphael R. Andonie, ARTORG Center for Biomedical Engineering Research, Murtenstrasse 50, Bern 3008, Switzerland. E-mail: raphael.andonie@unibe.ch

Received July 14, 2024; accepted January 15, 2025; published online ahead of print February 26, 2025

REFERENCES

Abbas, P. J., Tejani, V. D., Scheperle, R. A., Brown, C. J. (2017). Using neural response telemetry to monitor physiological responses to acoustic stimulation in hybrid cochlear implant users. *Ear Hear*, *38*, 409–425.

Alexiades, G., Dhanasingh, A., Jolly, C. (2015). Method to estimate the complete and two-turn cochlear duct length. *Otol Neurotol*, *36*, 904–907.

Alshalan, A., Abdelsamad, Y., Assiri, M., Alsanosi, A. (2022). Cochlear implantation: The variation in cochlear height. *Ear Nose Throat J*, *0*, 1455613221134860.

Andonie, R., Wimmer, W., Schraivogel, S., Mantokoudis, G., Caversaccio, M., Weder, S. (2024). Electrocochleography in cochlear implant recipients: Correlating maximum response with residual hearing. *Ear Hear*, *1*, 16.

Andonie, R. R., Wimmer, W., Wildhaber, R. A., Caversaccio, M., Weder, S. (2023). Real-time feature extraction from electrocochleography with impedance measurements during cochlear implantation using linear state-space models. *IEEE Trans Biomed Eng*, *70*, 3137–3146.

Békésy, G. V. (1960). *Experiments in Hearing*. McGraw-Hill Series in Psychology. McGraw-Hill.

Békésy, G. V. (2005). Hearing theories and complex sounds. *J Acoust Soc Am*, *35*, 588–601.

Bekesy, G. V. (1943). Über die Resonanzkurve und die Abklingzeit der verschiedenen Stellen der Schneckentrennwand. *Akust. Z*, *8*, 66-76.

Bester, C. W., Campbell, L., Dragovic, A., Collins, A., O'Leary, S. J. (2017). Characterizing electrocochleography in cochlear implant recipients with residual low-frequency hearing. *Front Neurosci*, *11*, 141.

Bester, C., Collins, A., Razmovski, T., Weder, S., Briggs, R. J., Wei, B., Zakaria, A. F., Gerard, J. -M., Mitchell-Innes, A., Tykocinski, M., Kennedy, R., Iseli, C., Dahm, M., Ellul, S., O'Leary, S. (2022). Electrocochleography triggered intervention successfully preserves residual hearing during cochlear implantation: Results of a randomised clinical trial. *Hear Res*, *426*, 108353.

Bester, C., Dalbert, A., Collins, A., Razmovski, T., Gerard, J. M., O'Leary, S. (2023). Electrocochleographic patterns predicting increased impedances and hearing loss after cochlear implantation. *Ear Hear*, *44*, 710–720.

Bester, C., Weder, S., Collins, A., Dragovic, A., Brody, K., Hampson, A., O'Leary, S. (2020). Cochlear microphonic latency predicts outer hair cell function in animal models and clinical populations. *Hear Res*, *398*, 108094.

Calloway, N. H., Fitzpatrick, D. C., Campbell, A. P., Iseli, C., Pulver, S., Buchman, C. A., Adunka, O. F. (2014). Intracochlear electrocochleography during cochlear implantation. *Otol Neurotol*, *35*, 1451–1457.

Campbell, L., Bester, C., Iseli, C., Sly, D., Dragovic, A., Gummer, A. W., O'Leary, S. (2017). Electrophysiological evidence of the basilar-membrane travelling wave and frequency place coding of sound in cochlear implant recipients. *Audiol Neurootol*, *22*, 180–189.

Carlson, M. L. (2020). Cochlear implantation in adults. *N Engl J Med*, *382*, 1531–1542.

Choudhury, B., Adunka, O. F., Demason, C. E., Ahmad, F. I., Buchman, C. A., Fitzpatrick, D. C. (2011). Detection of intracochlear damage with cochlear implantation in a gerbil model of hearing loss. *Otol Neurotol*, *32*, 1370–1378.

Dalbert, A., Pfiffner, F., Sli, C., Thoele, K., Sim, J. H., Gerig, R., Huber, A. M. (2015). Extra- and intracochlear electrocochleography in cochlear implant recipients. *Audiol Neurootol*, *20*, 339–348.

Dallos, P., & Cheatham, M. A. (1971). Travel time in the cochlea and its determination from cochlear-microphonic data. *J Acoust Soc Am*, *49*(Suppl 2), 1140–1143.

Dallos, P., & Cheatham, M. A. (1976). Production of cochlear potentials by inner and outer hair cells. *J Acoust Soc Am*, *60*, 510–512.

Eggermont, J. J. (1979). Narrow-band AP latencies in normal and recruiting human ears. *J Acoust Soc Am*, *65*, 463–470.

Forgues, M., Koehn, H. A., Dunnon, A. K., Pulver, S. H., Buchman, C. A., Adunka, O. F., Fitzpatrick, D. C. (2014). Distinguishing hair cell from neural potentials recorded at the round window. *J Neurophysiol*, *111*, 580–593.

Gantz, B. J., Hansen, M., Dunn, C. C. (2022). Review: Clinical perspective on hearing preservation in cochlear implantation, the University of Iowa experience. *Hear Res*, *426*, 108487.

Giardina, C. K., Brown, K. D., Adunka, O. F., Buchman, C. A., Hutson, K. A., Pillsbury, H. C., Fitzpatrick, D. C. (2019). Intracochlear electrocochleography: Response patterns during cochlear implantation and hearing preservation. *Ear Hear*, *40*, 833–848.

Giardina, C. K., Khan, T. E., Pulver, S. H., Adunka, O. F., Buchman, C. A., Brown, K. D., Pillsbury, H. C., Fitzpatrick, D. C. (2018). Response changes during insertion of a cochlear implant using extracochlear electrocochleography. *Ear Hear*, *39*, 1146–1156.

Gifford, R. H., Dorman, M. F., Skarzynski, H., Lorens, A., Polak, M., Driscoll, C. L., Roland, P., Buchman, C. A. (2013). Cochlear implantation with hearing preservation yields significant benefit for speech recognition in complex listening environments. *Ear Hear*, *34*, 413–425.

Greenwood, D. D. (1990). A cochlear frequency-position function for several species–29 years later. *J Acoust Soc Am*, *87*, 2592–2605.

Hempel, J. M., Simon, F., ller, J. M. (2018). Extended applications for cochlear implantation. *Adv Otorhinolaryngol*, *81*, 74–80.

Janssen, T., Steinhoff, H. J., Böhnke, F. (1989). [Correlation of the latency shift and brain stem potentials in basocochlear hearing loss and the time course of the click stimulus-induced evoked wave in the cochlea]. *Laryngorhinootologie*, *68*, 379–382.

Koka, K., Riggs, W. J., Dwyer, R., Holder, J. T., Noble, J. H., Dawant, B. M., Ortmann, A., Valenzuela, C. V., Mattingly, J. K., Harris, M. M., O'Connell, B. P., Litvak, L. M., Adunka, O. F., Buchman, C. A., Labadie, R. F. (2018). Intra-cochlear electrocochleography during cochlear implant electrode insertion is predictive of final scalar location. *Otol Neurotol*, *39*, e654–e659.

Koka, K., Saoji, A. A., Litvak, L. M. (2017). Electrocochleography in cochlear implant recipients with residual hearing: comparison with audiometric thresholds. *Ear Hear*, *38*, e161–e167.

Lenarz, T., Buechner, A., Gantz, B., Hansen, M., Tejani, V. D., Labadie, R., O'Connell, B., Buchman, C. A., Valenzuela, C. V., Adunka, O. F., Harris, M. S., Riggs, W. J., Fitzpatrick, D., Koka, K. (2022). Relationship between intraoperative electrocochleography and hearing preservation. *Otol Neurotol*, *43*, e72–e78.

O'Leary, S., Briggs, R., Gerard, J. M., Iseli, C., Wei, B. P. C., Tari, S., Rousset, A., Bester, C. (2020). Intraoperative observational real-time electrocochleography as a predictor of hearing loss after cochlear implantation: 3 and 12 month outcomes. *Otol Neurotol*, *41*, 1222–1229.

O'Leary, S., Mylanus, E., Venail, F., Lenarz, T., Birman, C., Di Lella, F., Roland, J. T., Gantz, B., Beynon, A., Sicard, M., Buechner, A., Lai, W. K., Boccio, C., Choudhury, B., Tejani, V. D., Plant, K., English, R., Arts, R., Bester, C. (2022). Monitoring cochlear health with intracochlear electrocochleography during cochlear implantation: Findings from an International Clinical Investigation. *Ear Hear*, *44*, 358–370.

Olson, E. S., Duifhuis, H., Steele, C. R. (2012). Von Békésy and cochlear mechanics. *Hear Res*, *293*, 31–43.

Polak, M., Lorens, A., Walkowiak, A., Furmanek, M., Skarzynski, P. H., Skarzynski, H. (2022). In vivo basilar membrane time delays in humans. *Brain Sci*, *12*, 400.

Rathgeb, C., Demattè, M., Yacoub, A., Anschuetz, L., Wagner, F., Mantokoudis, G., Caversaccio, M., Wimmer, W. (2019). Clinical applicability of a preoperative angular insertion depth prediction method for cochlear implantation. *Otol Neurotol*, *40*, 1011–1017.

Robles, L., & Ruggero, M. A. (2001). Mechanics of the mammalian cochlea. *Physiol Rev*, *81*, 1305–1352.

Rohatgi, A. (2024). WebPlotDigitizer. https://automeris.io/WebPlotDigitizer.html.

Ruggero, M. A. (1994). Cochlear delays and traveling waves: comments on 'Experimental look at cochlear mechanics'. *Audiology*, *33*, 131–142.

Ruggero, M. A., & Rich, N. C. (1987). Timing of spike initiation in cochlear afferents: Dependence on site of innervation. *J Neurophysiol*, *58*, 379–403.

Ruggero, M. A., & Temchin, A. N. (2007). Similarity of traveling-wave delays in the hearing organs of humans and other tetrapods. *J Assoc Res Otolaryngol*, *8*, 153–166.

Russell, I. J., & Nilsen, K. E. (1997). The location of the cochlear amplifier: spatial representation of a single tone on the guinea pig basilar membrane. *Proceedings of the National Academy of Sciences*, *94*, 2660–2664.

Saoji, A. A., Graham, M. K., Adkins, W. J., Koka, K., Carlson, M. L., Neff, B. A., Driscoll, C. L. W., Fitzpatrick, D. C. (2023). Multi-frequency electrocochleography and electrode scan to identify electrode insertion trauma during cochlear implantation. *Brain Sci*, *13*, 330.

Schoonhoven, R., Prijs, V. F., Schneider, S. (2001). DPOAE group delays versus electrophysiological measures of cochlear delay in normal human ears. *J Acoust Soc Am*, *109*, 1503–1512.

Schraivogel, S., Aebischer, P., Wagner, F., Weder, S., Mantokoudis, G., Caversaccio, M., Wimmer, W. (2023a). Postoperative impedance-based estimation of cochlear implant electrode insertion depth. *Ear Hear*, *44*, 1379–1388.

Schraivogel, S., Aebischer, P., Weder, S., Caversaccio, M., Wimmer, W. (2023b). Cochlear implant electrode impedance subcomponents as biomarker for residual hearing. *Front Neurol*, *14*, 1183116.

Schuerch, K., Waser, M., Mantokoudis, G., Anschuetz, L., Caversaccio, M., Wimmer, W., Weder, S. (2022a). Increasing the reliability of real-time electrocochleography during cochlear implantation: A standardized guideline. *Eur Arch Otorhinolaryngol*, *279*, 4655–4665.

Schuerch, K., Waser, M., Mantokoudis, G., Anschuetz, L., Wimmer, W., Caversaccio, M., Weder, S. (2022b). Performing intracochlear electrocochleography during cochlear implantation. *J Vis Exp*, *181*, e63153.

Schuerch, K., Wimmer, W., Dalbert, A., Rummel, C., Caversaccio, M., Mantokoudis, G., Weder, S. (2022c). Objectification of intracochlear electrocochleography using machine learning. *Front Neurol*, *13*, 943816.

Schuerch, K., Wimmer, W., Rummel, C., Caversaccio, M. D., Weder, S. (2023). Objective evaluation of intracochlear electrocochleography: Repeatability, thresholds, and tonotopic patterns. *Front Neurol*, *14*, 1181539.

Schurzig, D., Timm, M. E., Batsoulis, C., Salcher, R., Sieber, D., Jolly, C., Lenarz, T., Zoka-Assadi, M. (2018). A novel method for clinical cochlear duct length estimation toward patient-specific cochlear implant selection. *OTO Open*, *2*, 2473974–X18800238.

Seabold, S., & Perktold, J. (2010). Statsmodels: Econometric and statistical modeling with Python. In 9th Python in Science Conference. 92–96.

Sheffield, S. W., Jahn, K., Gifford, R. H. (2015). Preserved acoustic hearing in cochlear implantation improves speech perception. *J Am Acad Audiol*, *26*, 145–154.

Sijgers, L., Sorensen, T., Soulby, A., Boyle, P., Dalbert, A., sli, C., Jablonski, G. E., et al. (2023). Classification of acoustic hearing preservation after cochlear implantation using electrocochleography. *Trends Hear*, *27*, 23312165231220997.

Skarzynski, H., Lorens, A., Matusiak, M., Porowski, M., Skarzynski, P. H., & James, C. J. (2014). Cochlear implantation with the nucleus slim straight electrode in subjects with residual low-frequency hearing. *Ear hear*, *35*, e33–e43.

Teschner, M., Lenarz, T., Battmer, R. D. (2012). Validity of cochlear microphonics at high sound pressure levels as an important clinical aspect. *ORL J Otorhinolaryngol Relat Spec*, *74*, 38–41.

Verbist, B. M., Skinner, M. W., Cohen, L. T., Leake, P. A., James, C., Holden, C. ,T. A., et al. (2010). Consensus panel on a cochlear coordinate system applicable in histologic, physiologic, and radiologic studies of the human cochlea. *Otol Neurotol*, *31*, 722–730.

Virtanen, P., Gommers, R., Oliphant, T. E., Haberland, M., Reddy, T., Cournapeau, D., Burovski, E., Peterson, P., Weckesser, W., Bright, J., van der Walt, S. J., Brett, M., Wilson, J., Millman, K. J., Mayorov, N., Nelson, A. R. J., Jones, E., Kern, R., Larson, E., Carey, C. J., van Mulbregt P. SciPy 1.0 Contributors. (2020). SciPy 1.0: Fundamental algorithms for scientific computing in python. *Nat Methods*, *17*, 261–272.

Weder, S., Bester, C., Collins, A., Shaul, C., Briggs, R. J., O'Leary, S. (2020). Toward a better understanding of electrocochleography. *Ear Hear*, *41*, 1560–1567.

Weder, S., Bester, C., Collins, A., Shaul, C., Briggs, R. J., O'Leary, S. (2021). Real time monitoring during cochlear implantation: Increasing

the accuracy of predicting residual hearing outcomes. *Otol Neurotol*, *42*, e1030–e1036.

Wildhaber, R. A., Zalmai, N., Jacomet, M., Loeliger, H. -A. (2018). Windowed state-space filters for signal detection and separation. *IEEE Trans Signal Process*, *66*, 3768–3783.

Wimmer, W., de Oliveira, J. V., Breitsprecher, T. M., Hans, S., Van Rompaey, V., Van de Heyning, P., Dazert, S., Weiss, N. M. (2024). Metronome-guided cochlear implantation for slower and smoother insertions of lateral wall electrodes. *Eur Arch Otorhinolaryngol*, *281*, 4603–4609.

Wimmer, W., Vandersteen, C., Guevara, N., Caversaccio, M., Delingette, H. (2019). Robust cochlear modiolar axis detection in Ct. In International Conference on Medical Image Computing and Computer-Assisted Intervention, 3–10. Springer.

Yin, L. X., Barnes, J. H., Saoji, A. A., Carlson, M. L. (2021). Clinical utility of intraoperative electrocochleography (ECochG) during cochlear implantation: A systematic review and quantitative analysis. *Otol Neurotol*, *42*, 363–371.

Zeng, F. G. (2022). Celebrating the one millionth cochlear implant. *JASA Express Lett*, *2*, 077201.